Decimetric spike bursts versus microwave continuum

Gregory D. Fleishman [1,2,3], Dale E. Gary [2]

and

Gelu M. Nita [2]

ABSTRACT

We analyze properties of decimetric spike bursts occurring simultaneously with microwave gyrosynchrotron continuum bursts. We found that all of the accompanying microwave bursts were highly polarized in the optically thin range. The sense of polarization of the spike clusters is typically the same as the optically thin gyrosynchrotron emission, implying preferential extraordinary-wave-mode spike polarization. Optically thick spectral indices of the continuum were not observed to be larger than 2.5, suggesting low or absent Razin suppression. We find that the plasma frequency to gyrofrequency ratio is systematically lower in the spike-producing bursts compared to other bursts. The spike cluster flux density is found to be tightly correlated with the high-frequency spectral index of the microwave continuum for each event, while the flux-to-flux correlation may not be present. We discovered strong evidence that the trapped fast electrons producing the microwave gyrosynchrotron continuum have an anisotropic pitch-angle distribution of the loss-cone type in the spike-producing bursts. The spike clusters are mainly generated when the trapped electrons have the hardest and the most anisotropic distributions. The new properties are discussed against the currently available ideas about emission processes and models for spike generation. We conclude that the findings strongly support the electron cyclotron maser mechanism of spike emission, with characteristics agreeing with expectations from the local-trap model.

Subject headings: Sun: particle acceleration — Sun: flares — Sun: radio radiation

---

[1]Purple Mountain Observatory, National Astronomical Observatories, Nanjing 210008, P.R. China

[2]New Jersey Institute of Technology, Newark 07102 NJ, USA

[3]Ioffe Institute for Physics and Technology, 194021 St.Petersburg, Russia

1. Introduction

Millisecond solar radio spikes represent an interesting class of solar radio emission associated with flares. The spikes usually form a cluster of short-duration narrowband pulses on the dynamic spectrum covering a range of about a few hundreds MHz and lasting about a few minutes. This type of radio emission was initially interpreted as a signature of highly fragmented energy release in flares (Benz 1985). This idea had been one of the main "drivers" of the extensive observational (Benz et al 1982; Karlicky 1984; Messerotti et al.1985; Stähli and Magun 1986; Benz and Güdel 1987; Güdel 1990; Gary et al. 1991; Güdel et al. 1991; Csillaghy and Benz 1993; Altyntsev et al. 1995; Altyntsev et al. 1996; Karlicky et al. 1 Zlobec and Karlicky 1998; Wang et al. 2000) and theoretical (Stepanov 1978; Kuijpers et al 1981; Sharma et al. 1982; Sharma and Vlahos 1984; Li 1986; Winglee and Dulk 1986; Huang 1987; Winglee et al. 1988; Aschwanden 1990; Fleishman 1994; Fleishman and Yastrebov 1994b; Ledenev 1998; Stupp 2000; Barta and Karlicky 2001; Vlasov et al. 2002) studies of the subject.

However, the integrated spike flux was found to be delayed by $2-5$ s in respect to simultaneous hard X-ray (HXR) peaks (Aschwanden and Güdel 1992). This discovery is entirely inconsistent with the interpretation of the radio spikes as tracers of the primary energy release. Such a delay can be consistently explained in terms of spectral hardening of the respective fast electrons trapped in a coronal magnetic loop (Fleishman and Melnikov 1998). Respectively, this model associates the appearence of the spikes with a secondary fragmentation of the radio source (related, e.g., to the local inhomogeneities of the magnetic field).

Another important driver for the spike study is the strong diagnostic potential of the spikes related, e.g., to their extremely narrow bandwidth and short duration (Benz 1986). As a result, many important properties of the spikes have been established from the analysis of observations, leading to the development of many models. Currently, the most detailed comparison of the observed spike properties with various theoretical models is done in a recent review paper (Fleishman and Melnikov 1998). It was shown that the complete list of the spike properties can be interpreted within electron cyclotron maser (ECM) emission produced by fast electrons (with $E_{kin} \sim 10-100\ keV$) with a power-law momentum and anisotropic (loss-cone) pitch-angle distributions. The source of a spike cluster is shown to be a loop with more or less strong local inhomogeneities forming some local traps, where the pitch-angle anisotropy is stronger than on average and provides strong local wave amplification due to negative gyrosynchrotron absorption. Thus, each local trap forms a site where a single spike is generated.

The model has since been developed further to account for some specific spike properties. For example, quasilinear saturation of ECM (Fleishman and Arzner 2000) was shown to provide spike time profiles with a gaussian rise phase and exponential decay phase in agreement with spike observations (Güdel and Benz 1990; Fleishman and Melnikov 1998; Meszarosova et al. 2002). Non-integer harmonic ratios of the spikes (Krucker and Benz 1994) were interpreted as a result of an ECM line splitting due to source inhomogeneity (Fleishman and Platonov Platonov and Fleishman 2001).

Nevertheless, in spite of success of current models based on the ECM mechanism, the interpretation remains rather indirect, thus, more direct evidence for ECM operation in the spike bursts is strongly required.

According to ECM theory (Sharma et al. 1982; Sharma and Vlahos 1984; Li 1986; Winglee and Dulk Huang 1987; Aschwanden 1990; Fleishman and Yastrebov 1994a; Fleishman and Melnikov 1998; Stupp 2000) this mechanism is effective if

1. gyrofrequency to plasma frequency ratio is sufficiently large,

$$\omega_{Be}/\omega_{pe} \gtrsim 1, \tag{1}$$

2. the distribution function of fast electrons over momentum is sufficiently hard in the range of tens to hundreds keV,

3. the pitch-angle distribution of fast electrons is anisotropic (say, of loss-cone type).

There are various scenarios of ECM operation in solar flares. One of the widely accepted ideas assumes that the main population of fast electrons trapped in a loop is isotropic, while a minor fraction of the electrons just reflected up at the foot-points forms the loss-cone distribution providing the cyclotron instability. Therefore, these models predict that the spikes are generated in a restricted area around the foot-points.

We envision another possibility. If the main electron distribution has an anisotropic pitch-angle distribution (close to marginal stability state) then fluctuations of the angular distribution can provide ECM emission at any location through the entire loop. This model allows spikes to be generated at any height. Moreover, the overall anisotropy will substantially affect the accompanying incoherent gyrosynchrotron emission (Fleishman and Melnikov 2003), which can be tested observationally.

In particular, the model developed by (Fleishman and Melnikov 1998) assumes that the spikes are generated by a population of fast electrons accumulated in a magnetic loop due to formation of small-scale traps by inhomogeneities of the magnetic field. Gyrosynchrotron continuum bursts are known to be produced by trapped electrons as well (with characteristic electron energies from hundreds of keV to a few MeV).

Thus, the microwave continuum and simultaneous spike bursts should be related to each other. Since the properties of the gyrosynchrotron emission and its relation to the source parameters and fast electron distribution are well-known, we expect that analysis of some important correlations between spike bursts and gyrosynchrotron bursts might be rather informative to the study of solar radio spikes.

The study of spike cluster to microwave continuum correlations performed in this paper is similar to some extent to that done by (Aschwanden and Güdel 1992) who considered the correlations between spike clusters and HXR emission. Unlike that study, however, we pay a particular attention to the spectral properties of the microwave bursts (rather than flux-to-flux correlations only) and their association to energetic and pitch-angle distributions of the trapped fast electrons.

While both HXR and microwave emissions are produced by accelerated electrons with incoherent emission mechanisms, we emphasize that the study of spike-to-microwave correlations is not a simple repetition of the previous spike-to-HXR study for a few reasons. HXRs are produced mainly by precipitating electrons, while gyrosynchrotron emission is by trapped electrons. Thus, these are different (while related) populations of accelerated electrons. Also, the characteristic energies of radiating electrons are different for these two emission types. And finally, the gyrosynchrotron emission is sensitive to the coronal magnetic field and plasma density, unlike HXR.

We found that all of the conditions required for ECM generation are fulfilled in the analysed spike events, which is strong evidence that the spikes are produced by the ECM mechanism. Thus, the spike emission can be further used for more reliable diagnostics of the source parameters. In particular, we conclude that the spike clusters are associated with the flares that have the largest magnetic field (more specifically, the largest ω_{Be}/ω_{pe} ratio).

The paper is arranged as follows. Section 2 discusses briefly the observations and the selection criteria. Section 3 considers the theoretical concepts to be checked against the observations. Section 4 analyzes in some detail a few spike events recorded by Owens Valley Solar Array (OVSA) during 2001. Finally, the results are discussed in Section 5.

2. Observations

The Owens Valley Solar Array (OVSA), (Hurford et al. 1984; Gary & Hurford 1994), observes in the frequency range $1 - 18$ GHz, typically with 40 frequency channels. The standard temporal resolution is 4 s for the total intensity and 8 s for the circular polarization. The temporal resolution is obviously insufficient to resolve any single spike, since the typical spike duration is of the order of 10 ms or less in the frequency range $1-3$ GHz (Güdel and Benz 1990; Meszarosova et al. 2002). Nevertheless, an averaged flux of a dense spike cluster can be observed with the OVSA resolution. The results we describe here pertain to average properties of such spike clusters. In particular, the average spike flux densities likely relate more closely to the spike occurrence rate than to individual spike flux densities (Aschwanden and Güdel 1992).

For the detailed analysis we selected a few events demonstrating fluctuating low-frequency ($1-3.4$ GHz) emission with time scales much less than the time scales of the simultaneous microwave continuum. Only the events with narrowband decimetric structures and without any indication of drifting structures (such as could be related to type III bursts) were selected. Also, we did not include the events with very few decimetric peaks, since no quantitative analysis was possible for those cases. Finally, we selected six events (from about ten spike events recorded for the entire year 2001). Five of them were observed with the standard 4/8 s time resolution, while the sixth was with 2 s time resolution without polarization measurements.

3. Theoretical background

In essense, ECM is a kind of gyrosynchrotron emission in the conditions where the respective absorption coefficient is negative, providing wave amplification instead of absorption. Respectively, the usual solution for the radiation intensity applies for this case (for a uniform source):

$$J_\sigma(\omega,\vartheta)=\frac{j_\sigma(\omega,\vartheta)}{\varkappa_\sigma(\omega,\vartheta)}(1-e^{-\tau_\sigma}) \tag{2}$$

where $\tau_\sigma=\varkappa_\sigma L$ is the optical depth of the source for either ordinary ($\sigma=1$) or extraordinary ($\sigma=-1$) modes of radiation, L is the source size along the line of sight, $j_\sigma(\omega,\vartheta)$, $\varkappa_\sigma(\omega,\vartheta)$ are the emissivity and absorption coefficient of the gyrosynchrotron emission at frequency ω and viewing angle ϑ.

If the optical depth $|\tau|$ is large in value and positive, we arrive at the standard optically thick gyrosynchrotron emission, with the intensity

$$J_\sigma^{thick}(\omega,\vartheta)=\frac{j_\sigma(\omega,\vartheta)}{\varkappa_\sigma(\omega,\vartheta)}, \tag{3}$$

whose spectral behavior does not depend noticeably on the electron spectral index.

However, if the absorption coefficient is negative for some restricted range of the frequency and viewing angle for any wave-mode, the amplification of the respective waves occurs according to Eq. (2), which reduces to

$$J_\sigma^{ECM}(\omega,\vartheta)=\frac{j_\sigma(\omega,\vartheta)}{|\varkappa_\sigma(\omega,\vartheta)|}e^{|\tau_\sigma|} \tag{4}$$

if $|\tau_\sigma| >> 1$ for this case (in the linear approximation).

From these two equations it becomes very clear what kind of correlation should exist in observations when we compare ECM emission with the standard gyrosynchrotron emission. The ratio of the two becomes

$$J_\sigma^{ECM}(\omega_1,\vartheta)/J_\sigma^{thick}(\omega_2,\vartheta)=\frac{j_\sigma(\omega_1,\vartheta)/|\varkappa_\sigma(\omega_1,\vartheta)|}{j_\sigma(\omega_2,\vartheta)/\varkappa_\sigma(\omega_2,\vartheta)}e^{|\tau_\sigma|}, \tag{5}$$

where ω_1 is the (low) frequency at which ECM emission is generated, ω_2 is a (higher) frequency at which the gyrosynchrotron source is optically thick, and $|\tau_\sigma|$ is the optical depth of the ECM emission. The ratio depends primarily on the exponential factor $e^{|\tau_\sigma|}$ while the pre-exponential factor has much weaker dependence on the distribution function of fast electrons (Fleishman and Melnikov 2003). Thus, the logarithm of the ratio (5) is linearly related to the optical depth $|\tau_\sigma|$, which in turn depends substantially on the distribution function of fast electrons.

More specifically (Fleishman and Yastrebov 1994a; Fleishman and Melnikov 1998), the negative absorption coefficient (and $|\tau_\sigma|$ respectively) increases in value as the hardness of the electron momentum spectrum and pitch-angle anisotropy (namely, the angular gradient) of the loss-cone distribution increase. On the other hand, the hardness and the pitch-angle distribution specify the optically thin spectral index of the incoherent gyrosynchrotron radiation (Ramaty 1969; Fleishman and Melnikov 2003).

The calculations of the standard gyrosynchrotron emission produced by anisotropic pitch-angle distributions of fast electrons with a power-law momentum distribution (Fleishman and Melnikov show that the optically thin spectral index (α_h) of the gyrosynchrotron radiation depends substantially on the viewing angle at which the gyrosynchrotron source is observed with respect to the magnetic field. For the quasitransverse case, the spectral index is specified primarily by the spectral index δ of the fast electron distribution over momentum, so that harder electron distributions produce flatter gyrosynchrotron spectra in the optically thin region. However, for the quasiparallel case (Fleishman and Melnikov 2003), the spectral index α_h is specified mainly by the pitch-angle anisotropy of fast electrons in such a way that more anisotropic distributions produce softer optically thin gyrosynchrotron spectra (larger α_h).

Thus, combining the predictions of the ECM and gyrosynchrotron theories, we can expect two different types of correlation between $|\tau_\sigma|$ and α_h. If we observe the microwave source at a quasitransverse direction, then the larger optical depth $|\tau_\sigma|$ should correspond to a flatter gyrosynchrotron spectrum in the optically thin region, while for the quasiparallel case the larger optical depth $|\tau_\sigma|$ should correspond to a steeper gyrosynchrotron spectrum.

4. Data analysis

(Aschwanden and Güdel 1992) considered correlations between decimetric spike rate, integrated over some frequency range, and HXR emission. In particular, they found that some X-ray peaks are tightly correlated with the averaged spike flux density, while others are entirely uncorrelated. This was interpreted (but not proven) as a result of particle acceleration in different loops with only part (one) of them satisfying the specific conditions for the spike generation. Another important finding is a considerable time delay (of $2-5$ s) of the averaged spike flux in respect to HXR peaks.

Accordingly, we performed some studies similar (and complementary) to those by (Aschwanden and Gü but we paid more attention to the role of gyrosynchrotron spectral evolution based on the theoretical concepts discussed briefly in Section 3.

First of all, we address the question if there are any indications that the ratio of frequencies (1) is systematically larger for bursts producing the spike clusters than on average for all radio bursts. For this purpose we study the low-frequency part of the microwave continuum bursts. It is well-known (Bastian et al. 1998; Fleishman and Melnikov 2003) that the slope (α_l) of the low-frequency gyrosynchrotron emission depends on the gyrofrequency to plasma frequency ratio due to the Razin effect. While the expected low-frequency spectral indices for the gyrosynchrotron optical depth is $\alpha_l < 3$, the Razin effect can increase the values to the range $\alpha_l > 3$ if $\omega_{Be}/\omega_{pe} < 0.3$.

Figure 1 displays the distribution of the low-frequency spectral indices α_l separately for the spike-producing bursts and all other gyrosynchrotron bursts. It is remarkable that the overall distribution has a significant tail in the range $\alpha_l > 3$, while the spike-producing bursts display the spectral indices lying entirely in the range $\alpha_l < 2.5$. Thus, no indication of the Razin-effect operating in the spike-producing bursts is present, hence, we can conclude the condition (1) is fulfilled for these events.

Below we analyze in more detail the six events with dense spike clusters in the range $1.2-3.4$ GHz, recorded by OVSA during 2001.

4.1. 25-mar-01 event

The event lasted about 8 min, Figure 2*a*, the microwave continuum burst produced a flux density up to 50 sfu, while the decimetric flux density exceeded 150 sfu. The power and polarization spectra, averaged over the entire burst duration, are shown in Figure $2b, c$. The microwave burst displays a remarkably strong degree of polarization at the high (optically thin) frequencies. A few important conclusions can be derived from the polarization plot. First, the microwave source is reasonably uniform, otherwise, the degree of polarization might not have been so strong. Second, we look at the source at a direction quasiparallel to the magnetic field, since at a quasitransverse direction even a uniform source would produce a weak or moderate degree of polarization. Third, the dominant sense of circular polarization (L) for the spikes is that expected for optically thin gyrosynchrotron emission (X-mode) and opposite to that of optically thick emission (typically, O-mode). Thus, the spikes are preferentially X-mode polarized (within the simplest geometry). We have to emphasize that we discuss here an averaged degree of polarization of the entire spike cluster, while the instantaneous degree of polarization varies with time and can be as large as 100%. The sense of spike polarization also changes with time. Moreover, the preferential sense of spike polarization depends on frequency: lower-frequency spikes ($1.2 - 2$ GHz) are mainly L-polarized, while higher-frequency spikes ($2 - 3.4$ GHz) are mainly R-polarized.

Let us proceed to examine correlations between spike emission and microwave continuum. Figure 3*a* displays a very good correlation between averaged spike flux and microwave light curve. This finding is similar to that found for HXR bursts accompanied by spike clusters: some HXR peaks are tightly correlated with the spike rate (Aschwanden and Güdel 1992). (Aschwanden and Güdel 1992) found that the averaged spike flux is delayed by $2 - 5$ s with respect to the simultaneous HXR peak, which was further interpreted as a result of trapping and consequent spectral evolution of spike-generating fast electrons (Fleishman and Melnikov 1998), while the HXR peak is caused mainly by precipitating electrons.

Figure 3*b* displays the dependence of the cross-correlation coefficient between the spike flux density integrated over the low-frequency band and the gyrosynchrotron flux density at a selected (optically thick) frequency as a function of the respective time lag. The respective spline fit (solid curve) has a maximum at $\Delta t \approx 2.5$ s, accordingly, the *optically thick* gyrosynchrotron emission is delayed by 2.5 s with respect to spike emission. Indeed, the delay value is frequency dependent in agreement with the property of the microwave bursts (Melnikov and Magun 1998), but the sign is stable. Since both types of radio emission are produced by trapped electrons, the delay can be easily interpreted if the spike emission is produced by fast electrons of lower energy than the gyrosynchrotron emission, because the characteristic lifetime of the trapped electrons increases with the electron energy.

The theory described in Section 3 predicts a correlation between the (negative) optical depth in the spike frequency range and the gyrosynchrotron spectral index α_h in the optically thin range. To study this correlation we plot in Figure 3*c* the quantity $\log(F_{thick}/F_{spike})$ versus high-frequency microwave spectral index α_h, where F_{thick} is the gyrosynchrotron flux density at an optically thick frequency, namely $f = 6.6$ GHz, and F_{spike} is the spike flux density integrated from 1.2 GHz to 3.4 GHz. The respective correlation coefficient is remarkably large, $R = 0.73$. The positive slope of the regression means that spikes are preferentially generated when the optically thin gyrosynchrotron emission displays the softest spectrum, which (for the quasiparallel viewing angle) corresponds to the most anisotropic pitch-angle distributions of the fast electrons.

4.2. 24-aug-01 event

The event shown in Figure 4*a* is generally similar to the previous one but one order of magnitude stronger: the microwave peak flux is about 400 sfu, while the spike peak flux density is about 1500 sfu. The total and polarized flux density (Figure 4*b*) give rise to the averaged polarization spectrum shown in Figure 4*c*. The degree of polarization is exceedingly strong at the high (optically thin) frequencies, which is evidence for the quasiparallel viewing angle of the gyrosynchrotron source. It is interesting that the sense of polarization in the optically thick region is the same as in the optically thin region, which can be naturally interpreted as an effect of pitch-angle anisotropy of the radiating fast electrons (Fleishman and Melnikov 2003). The spikes are mainly polarized with the same sense, thus, we again arrive at the conclusion of the preferential X-mode polarization of the spikes.

The averaged spike and microwave fluxes display a significant correlation (Figure 5*a*) with the correlation coefficient $R = 0.72$. The microwave emission is delayed by about 9.6 s with respect to the spike emission (Figure 5*b*), which again is expected due to the energy dependent lifetime of the trapped fast electrons.

The logarithm of the ratio of the optically thick gyrosynchrotron flux density to the averaged spike flux density (Figure 5*c*) displays an especially tight correlation with the high-frequency microwave spectral index (Figure 5*e*) during a 3 min interval of the burst (from 20:38:10 to 20:41:20 UT), when a reliable spectral index data is available. Thus, we again conclude that the spikes are mainly generated during the softest microwave spectra. For the quasiparallel case, softer spectra indicate more anisotropic pitch-angle distributions of the fast electrons, hence, the spikes are produced most efficiently when the pitch-angle distribution of the trapped fast electrons is the most anisotropic.

4.3. 30-aug-01 event

The event lasted about 10 min (Figure 6*a*), but only the main phase (from 17:49:30 to 17:53:00) allows for the quantitative analysis requiring data of sufficiently high flux density. The peak flux densities of both microwave and spike emissions exceed 200 sfu in this event. The spikes display clustering on the frequency domain; we analyze here the properties of the spike flux integrated over the entire range from 1.2 GHz to 3.2 GHz. The average total and polarized spectrum (Figure 6*b*) provide us with the polarization spectrum (Figure 6*c*). The very large degree of polarization in the optically thin range allows us to derive that the microwave source is observed at a direction quasiparallel to the magnetic field similar to the previous two cases. The sense of polarization of the spike clusters is the same as that of the optically thin gyrosynchrotron emission, once again suggesting the preferential X-mode polarization of spikes.

The first microwave peak is well correlated with the integrated spike flux, while the second one displays a much weaker correlation, similar the findings of the spike-HXR correlation study (Aschwanden and Güdel 1992). For this reason, the flux-to-flux correlation is not quite so strong ($R = 0.66$) for the entire analyzed time segment (Figure 7*a*). The dependence of the correlation coefficient of the time lag (Figure 6*b*) shows that the microwave emission is delayed only slightly, if at all, with respect to spike emission.

The correlation between $\log(F_{thick}/F_{spike})$ and α_h remains significant, at $R = 0.49$, but is less than in two previous cases. Nevertheless, the general conclusion is the same for all three analyzed events demonstrating strong polarization of the optically thin gyrosynchrotron emission: the spikes are generated most efficiently when the gyrosynchrotron emission displays the softest spectra.

4.4. 05-oct-01 event

The spikes in this event lasted about 6 min, Figure 8*a*. This is the weakest of the analyzed events, the peak flux density of both microwave and spike bursts being below 100 sfu (Fig.8*b*).

The total and polarized flux data are reliable at $f < 10$ GHz (Figure 8*b*), above which the flux density becomes too low. The polarization spectrum displays a moderate degree of polarization ($P < 50\%$) in the optically thin region (Figure 8*c*). In essence, there are a few possibilities to provide such a moderate polarization of the gyrosynchrotron emission (e.g., a single source observed at a quasitransverse direction, superposition of two quasiparallel sources with opposite directions of the magnetic field, or a more complicated non-uniform source).

We, however, adopt the simplest model—a single gyrosynchrotron source—as we did for the three previous events. In this case the source is observed at a quasitransverse direction (to avoid very strong high-frequency polarization). One can note that the spikes above 1.6 GHz are polarized oppositely to the optically thin gyrosynchrotron emission, while below 1.6 GHz they have the same sense of polarization.

The averaged spike and microwave fluxes are entirely uncorrelated, $R = 0.13$, Figure 9*b*, although there is some indication that the microwave emission is delayed by 5.9 s with respect to the spike emission (Figure 9*b*). Nevertheless, the quantities $\log(F_{thick}/F_{spike})$ and α_h reveal a significant negative correlation, $R = -0.46$ (Figure 9*d*) implying a physical relation between these two emission types. The negative slope of the regression means that the spikes are generated most efficiently when the gyrosynchrotron emission displays the hardest spectra, in contrast to the case of the three previous bursts.

For the quasitransverse viewing angles the high-frequency slope is related primarily to the hardness of the fast electron momentum distribution. We, thus, conclude that the spikes are generated when the fast electrons have the hardest spectrum. A similar property was noted in the spike-HXR correlation study (Aschwanden and Güdel 1992).

4.5. 02-apr-01 event

This event (Figure 10*a*) is exceptionally strong. The microwave peak exceeded 1000 sfu, while the spike flux exceeded $3 \cdot 10^4$ sfu. The event lasted more than half an hour and produced a few spike clusters. We analyze them all together, which provides a very long time series that improves the statistical significance of the results.

The polarization of the optically thin gyrosynchrotron emission (Figure 6*c*) is moderate ($P < 60\%$), which is interpreted here (as the simplest assumption) as an effect of quasitransverse viewing angle of the gyrosynchrotron source. The polarization of spike clusters is rather strong, $P \sim 70 - 90\%$ on average, the sense of polarization is the same as for optically thin gyrosynchrotron emission. Thus, the spikes are preferentially X-mode polarized.

The microwave and integrated spike fluxes are remarkably uncorrelated (Figure 11a, b), at least on average (while some "tracks" can be noted in the plot). Accordingly, no delay between these two types of emission can be found reliably for this event.

However, if the spikes are produced by the ECM mechanism, the correlation between $\log(F_{thick}/F_{spike})$ and α_h *must* exist. Figure 11e, f displays this remarkable correlation ($R =$

−0.61) related to the entire duration of the event (more than half an hour!). The spikes are again generated when the gyrosynchrotron emission displays the hardest spectra, which, for the quasitransverse case, corresponds to the hardest spectra of the fast electrons.

4.6. 19-oct-01 event

This is one of the strongest events (Figure 12) recorded on 2001: the microwave peak exceeded 5000 sfu, while the spike flux exceeded $3 \cdot 10^4$ sfu (13*a*). The event was observed with a time resolution of 2 s, and we analysed the period during the first peak (first ~ 7 min) of the event, during which the spikes were obviously stronger than the competing low-frequency continuum emission.

The polarization data are unavailable with the fast mode, thus, we are limited to the total flux data for this event. There is general flux-to-flux correspondence for this case (Figure 13*c*) providing the correlation of $R = 0.85$ (Figure 13*d*). The microwave emission is delayed by 7.3 s with respect to the spike flux at $f = 1.2$ GHz. Unlike previous events, we did not integrate the decimetric flux over a few frequency channels, because the contribution of smoothed decimetric continuum component becomes important at higher frequencies (1.4 − 2 GHz) during parts of the burst.

The correlation between $\log(F_{thick}/F_{spike})$ and α_h is quite strong and negative for this case, $R = -0.79$ (Figure 13*d*). We note that the correlation between $\log(F_{thick}/F_{spike})$ and α_h remains negative until about half-way through the second gyrosynchrotron peak at $\sim$ 1631 UT, and then reverses to a positive correlation, which we believe is due to the spike emission giving way to a low-frequency continuum emission of another origin. Although spike clusters appear later in the burst, the gyrosynchrotron emission peaks at such a low frequency after about 1640 UT that we cannot obtain the optically thick flux density, and so cannot examine the correlation between $\log(F_{thick}/F_{spike})$ and α_h. Therefore, at least during the first 7 min of this event where the correlation can be performed, we can classify the event as being observed at a quasitransverse direction, similarly to two previous events, and we once again conclude that harder electron distributions are preferable for the spike generation.

5. Discussion

We analyzed in some detail six events producing dense spike clusters in the frequency range 1.2 − 3.4 GHz observed simultaneously with microwave gyrosynchrotron continuum.

A few new important findings are firmly established. First of all, the low-frequency part of the respective microwave bursts is considerably flatter than for the overall microwave event set. This means that there is no indication of the Razin effect operating in the microwave events accompanying the decimetric spike bursts. Consequently, the ratio ω_{Be}/ω_{pe} is large enough in the spike sources to allow operation of the ECM mechanism.

Secondly, all five events with polarization data available reveal a *high* degree of polarization in the optically thin gyrosynchrotron range significantly larger than typical mean value of $20\% \pm 16\%$ (Bruggmann and Magun 1990). This deviation is most probably related to the fast electron pitch-angle anisotropy (of the loss-cone type), which increases the degree of X-mode polarization compared with isotropic case (Fleishman and Melnikov 2003). Moreover, two of the analyzed events do not display a change of the sense of polarization from the thin to thick region, which might be related to the effect of the pitch-angle anisotropy as well (Fleishman and Melnikov 2003). Note that the high degree of polarization implies a rather non-symmetric magnetic structure at the source site, since a symmetric loop would give more equal fluxes in both polarizations, leading to smaller net polarization.

Thirdly, important information about the pitch-angle anisotropy of the radiating fast electrons can be obtained from the analysis of the distribution of the high-frequency microwave spectral indices. Figure 14a displays the distribution of spectral indices for the quasitransverse spike-producing bursts overplotted on the overall distribution for the gyrosynchrotron bursts above 60 sfu. The average hardness of spike-producing events is similar to that for all other events (however, one could note a lack of soft $\alpha_h < -3$ values for the spike-producing events). Since α_h is related to the fast electron momentum distribution for the quasitransverse case (Fleishman and Melnikov 2003), we can conclude that the spikes are produced by the electrons with more or less typical energy spectrum. However, for the quasiparallel case the pitch-angle anisotropy can provide much softer gyrosynchrotron spectra for the same electron energy spectrum. Figure 14b displays the distribution of the spectral indices for the quasiparallel spike-producing bursts overplotted on the overall distribution for the gyrosynchrotron bursts above 60 sfu. The respective gyrosynchrotron spectra are significantly softer than on average (one can note a strong excess in the range of $-7 < \alpha_h < -4$), which could only be ascribed to the effect of the pitch-angle anisotropy. This pitch-angle anisotropy is favourable to produce coherent ECM or plasma emission. However, the preferential X-mode polarization of the spikes together with the variations of the sense of polarization observed in many events are evidence of the ECM mechanism of spike production. The conclusion of the preferential X-mode polarization of the spikes agrees with the results of (Güdel and Zlobec 1991). Since the ECM mechanism allows for both modes to be generated (Stupp 2000), the finding of (Benz and Pianezzi 1997) that (for a selected set of spike observations) the original spikes are entirely O-mode polarized at their source is consistent with this model as well.

Fourthly, the analyzed events fall into two distinctive groups: those with a strong polarization of high-frequency gyrosynchrotron emission display a (positive) correlation between $\log(F_{thick}/F_{spike})$ and α_h, while those with a weaker polarization display a (negative) anti-correlation between these two quantities. We interpret this difference as an effect of viewing angle at which the gyrosynchrotron source is observed: strong polarization corresponds to a viewing angle quasiparallel to the magnetic field, while weaker polarization corresponds to the quasitransverse case. For the quasiparallel case, the gyrosynchrotron spectral index depends primarily on the pitch-angle anisotropy (Fleishman and Melnikov 2003), namely, it increases as the anisotropy increases. However, for the quasitransverse case, the effect of pitch-angle anisotropy on the spectral index is weak, and the spectral index is specified primarily by the electron energy distribution as for isotropic case. This interpretation of these two kinds of the correlation plots is pretty consistent with the distributions of the high-frequency spectral indices (Figure 14) discussed above.

From the entire set of data, we therefore conclude that the millisecond solar radio spikes are generated at a source with relatively high gyrofrequency to plasma frequency ratio, during that phase of the bursts when the trapped fast electrons have the hardest energy distribution and the most anisotropic pitch-angle distribution. These properties are naturally expected within ECM theory (Fleishman and Yastrebov 1994a), while meeting large difficulties within alternative theories based on various modifications of the plasma mechanism (Fleishman and Melnikov 1998). Moreover, the pitch-angle anisotropy of the trapped electrons suggested by the data is in favor of the local trap model (Fleishman and Melnikov 1998), while inconsistent with foot-point source models of spike generation.

The incoherent microwave emission is found to be delayed significantly (by $5-30$ s) with respect to averaged spike flux density. Combining this finding with the result of (Aschwanden and Güdel 1992) that the averaged spike flux is delayed by $2-5$ s in respect to simultaneous HXR peaks, we conclude that HXR emission arrives first, then the spike emission and finally the incoherent gyrosynchrotron emission. This sequence is related to underlying kinetics of fast electrons: the directly precipitating electrons produce HXR emission, low-energy trapped electrons produce spikes and higher-energy trapped electrons produce incoherent gyrosynchrotron emission. This is consistent with the delays (of a few seconds to a few tens of seconds) between HXR peaks and microwave bursts found earlier (Melnikov 1994).

(Aschwanden and Güdel 1992) found that sometimes there is very tight correlation between the averaged spike flux and the respective HXR flux, but sometimes there is no good flux-to-flux correlation. We found here the same property when considering the microwave emission in place of HXR emission. However, *each* spike-producing burst reveals a significant correlation between $\log(F_{thick}/F_{spike})$ and high-frequency slope α_h of the microwave gyrosynchrotron emission. This slope is related to the energy and pitch-angle distributions of the radiating fast electrons. We, thus, conclude that the spike production is directly related to the properties of the distribution function (over the momentum and pitch-angle) of the trapped electrons.

The derived properties of the distribution functions as well as source conditions (large ω_{Be}/ω_{pe} ratio) are found to be pretty consistent with those required for the ECM operation. We, therefore, can conclude that the performed study gives rise to new important evidence that millisecond solar radio spikes are produced by electron cyclotron maser mechanism.

Nevertheless, we feel that some important additional studies are necessary. For example, spatially resolved data are strongly desirable to locate the spike source in respect to the microwave source and to respective magnetic field. Also, the combined analysis of the spike, microwave and HXR bursts observed for the same events can be exceedingly helpful to constrain the involved parameters and use the spike emission for further diagnostic purposes. From this point of view, some additional work should be done to specify the gyroharmonics providing the main contribution to the radio spike emission.

Acknowledgements. The work was supported by NSF grant AST-9987366 and NASA grant NAG5-11875 to New Jersey Institute of Technology, the Russian Foundation for Basic Research, grants No.00-02-16356, 02-02-39005, and Chinese NFS projects No.10273025, “973” program with No.G2000078403.

REFERENCES

Altyntsev, A.T., Grechnev, V.V., Zubkova, G.N., Lesovoi, S.V., Lisysian, E.G., Treskov, T.A., Rosenraukh, Y.M, and Magun, A. 1995, A&A, 303, 249

Altyntsev, A.T., Grechnev, V.V., Konovalov, S.K., Lesovoi, S.V., Lisysian, E.G., Treskov, T.A., Rosenraukh, Y.M, and Magun, A. 1996, ApJ, 469, 976

Aschwanden, M.J. 1990, Astron. Astrophys. Suppl. 85, 1141

Aschwanden, M.J., and Güdel, M. 1992 ApJ, 401, 736

Barta, M., and Karlicky, M. 2001, A&A, 379, 1045

Bastian, T.S., Benz, A.O., and Gary, D.E. 1998, Annu. Rev. Astron. Astrophys., 36, 131

Benz, A.O. 1985, Sol. Phys., 96, 357

Benz, A.O. 1986, Sol. Phys., 104, 99

Benz, A.O., and Güdel M. 1987, Sol. Phys., 111, 175

Benz, A.O., and Pianezzi, P. 1997, A&A, 323, 250

Benz, A.O., Zlobec, P., and Jaeggi, M. 1982, A&A, 109, 305

Bruggmann, G., and Magun, A. 1990, A&A, 239, 347

Csillaghy, A., and Benz, A.O. 1993, A&A, 274, 487

Fleishman, G.D. 1994, Sol. Phys., 153, 367

Fleishman, G.D., and Arzner, K. 2000, A&A, 358, 776

Fleishman, G.D., and Melnikov, V.F. 1998, Physics - Uspekhi, 41, 1157

Fleishman, G.D., and Melnikov, V.F. 2003, ApJ, 587,

Fleishman, G.D., and Platonov, K.Yu. 1999, Proc. 9^{th} European Meeting on Solar Physics, "Magnetic Fields and Solar Processes", Florence, Italy, 12-18 September 1999. ESA SP-448, December 1999, 2, 809

Fleishman, G.D., and Yastrebov, S.G. 1994a, Solar Phys. 153, 389

Fleishman, G.D., and Yastrebov, S.G. 1994b, Sol. Phys., 154, 361

Gary, D.E., Hurford, G.J., and Flees, D.J. 1991, ApJ, 369, 255

Gary, D. E. & Hurford, G. J. 1994, ApJ, 420, 903

Güdel, M. 1990, A&A, 239, L1

Güdel, M., Aschwanden, M.J., and Benz, A.O. 1991, A&A, 251, 285

Güdel, M., and Benz, A.O. 1990, A&A, 231, 202

Güdel, M., and Zlobec, P. 1991, A&A, 245, 299

Huang, G.-L. 1987, Sol. Phys., 114, 363

Hurford, G. J., Read, R. B., & Zirin, H. 1984, Sol. Phys., 94, 413

Karlicky, M. 1984, Sol. Phys., 92, 329

Karlicky, M., Sobotka, M., and Jiricka, K. 1996, Sol. Phys., 168, 375

Krucker, S., and Benz A.O. 1994, A&A, 285, 1038

Kuijpers, J., Van der Post, P, and Slottje, C. 1981, A&A, 103, 331

Ledenev, V.G. 1998, Sol. Phys., 179, 405

Li, H.W. 1986, Sol. Phys.104, 131

Melnikov, V.F. 1994, Radiophys. Quantum Electron., 37, 557

Melnikov, V.F., and Magun, A. 1998, Sol. Phys., 178, 153

Messerotti, M., Nonino, M., and Zlobec, P. 1985, Met. S. A. It., 56, 795

Meszarosova, H., Veronig, A., Zlobec, P., and Karlicky, M. 2002 Proc. 10^{th} European Solar Physics Meeting, 'Solar Variability: From Core to Outer Frontiers', Prague, Czech Republic, 9-14 September 2002 (ESA SP-506, December 2002), 1, 347.

Platonov, K.Yu., and Fleishman, G.D. 2001, Astron. Zh., 78, 238 (transl.: Astronomy Repts., 45, 203)

Ramaty, R. 1969, ApJ, 158, 753

Sharma, R.R., and Vlahos, L. 1984, ApJ, 280, 405

Sharma, R.R., Vlahos, L., and Papadopoulos, K. 1982, A&A, 112, 377

Stähli, M., and Magun, A. 1986, Sol. Phys., 104, 117

Stepanov, A.V. 1978, Pis'ma v Astron. Zh., 4, 193

Stupp, A. 2000, MNRAS, 311, 251

Vlasov, V.G., Kuznetsov, A.A., and Altyntsev, A.T. 2002, A&A, 382, 361

Wang, M., Fu, Q., Xie, R., and Huang, G. 2000, Astroph. Repts., 36, 77

Winglee, R.R., and Dulk, G.A. 1986, Sol. Phys., 104, 93

Winglee, R.R., Dulk, G.A., and Pritchett, P.L. 1988, ApJ, 328, 809

Zlobec, P., and Karlicky, M. 1998, Sol. Phys., 182, 477

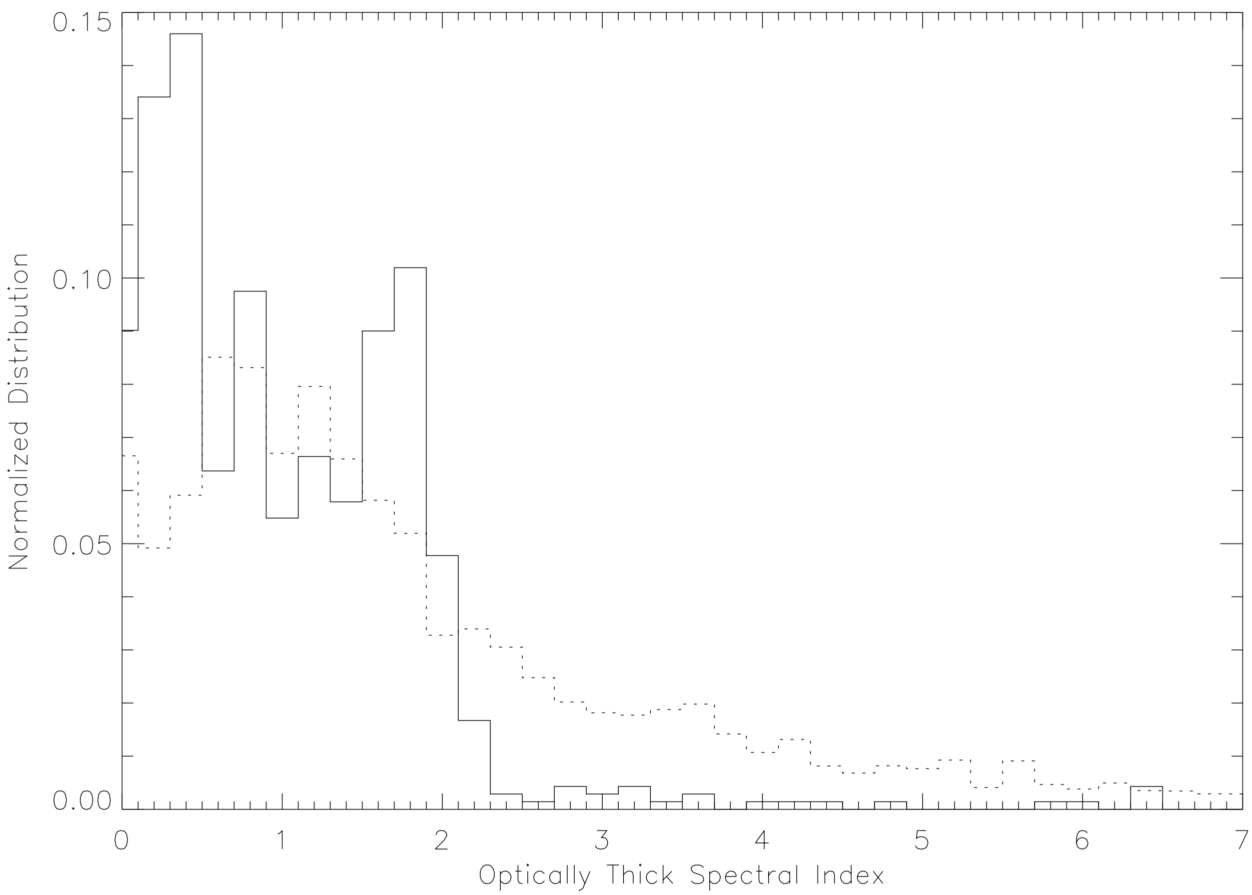

Fig. 1.— Distribution of optically thick spectral index of 6 spike-producing bursts (solid line) and the equivalent distribution obtained for 125 gyrosynchrotron bursts above 60 sfu observed by OVSA during 2001 (dashed line).

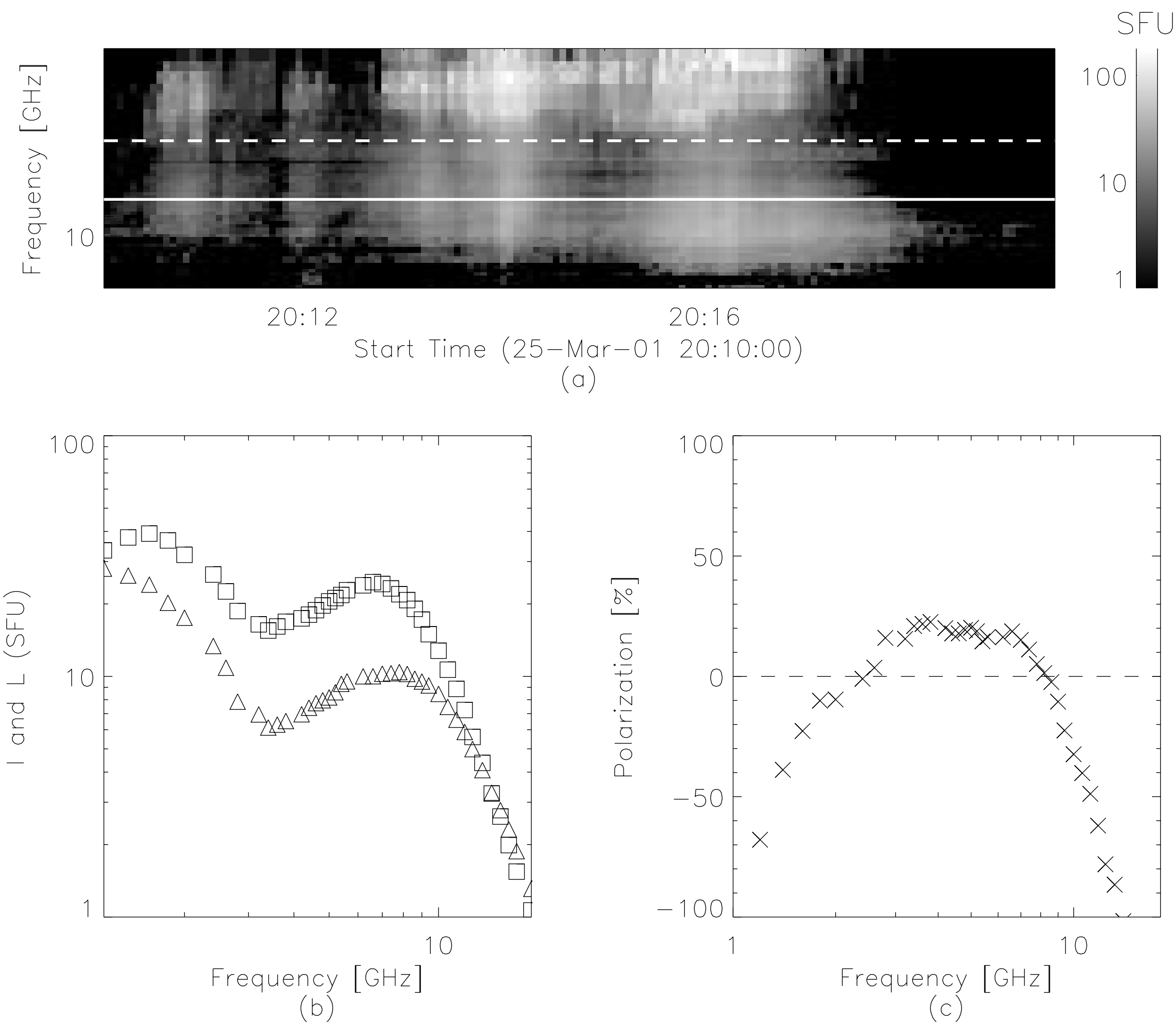

Fig. 2.— March 25, 2001: (a)-Dynamic spectrum recorded by OVSA at 40 frequencies between 1.2 and 18 GHz at 4 s time resolution. The solid line, 6.6 GHz, and the dashed line, 3.4 GHz, represent the optically thick frequency and, respectively, the upper integration limit of the spiky emission used to obtain the results displayed in Fig.3. (b)-The time averaged total power emission (squares) and Left-hand polarization data (triangles) for the same segment of time as in (a). (c)-The averaged polarization spectrum computed using the magnitudes displayed in (b).

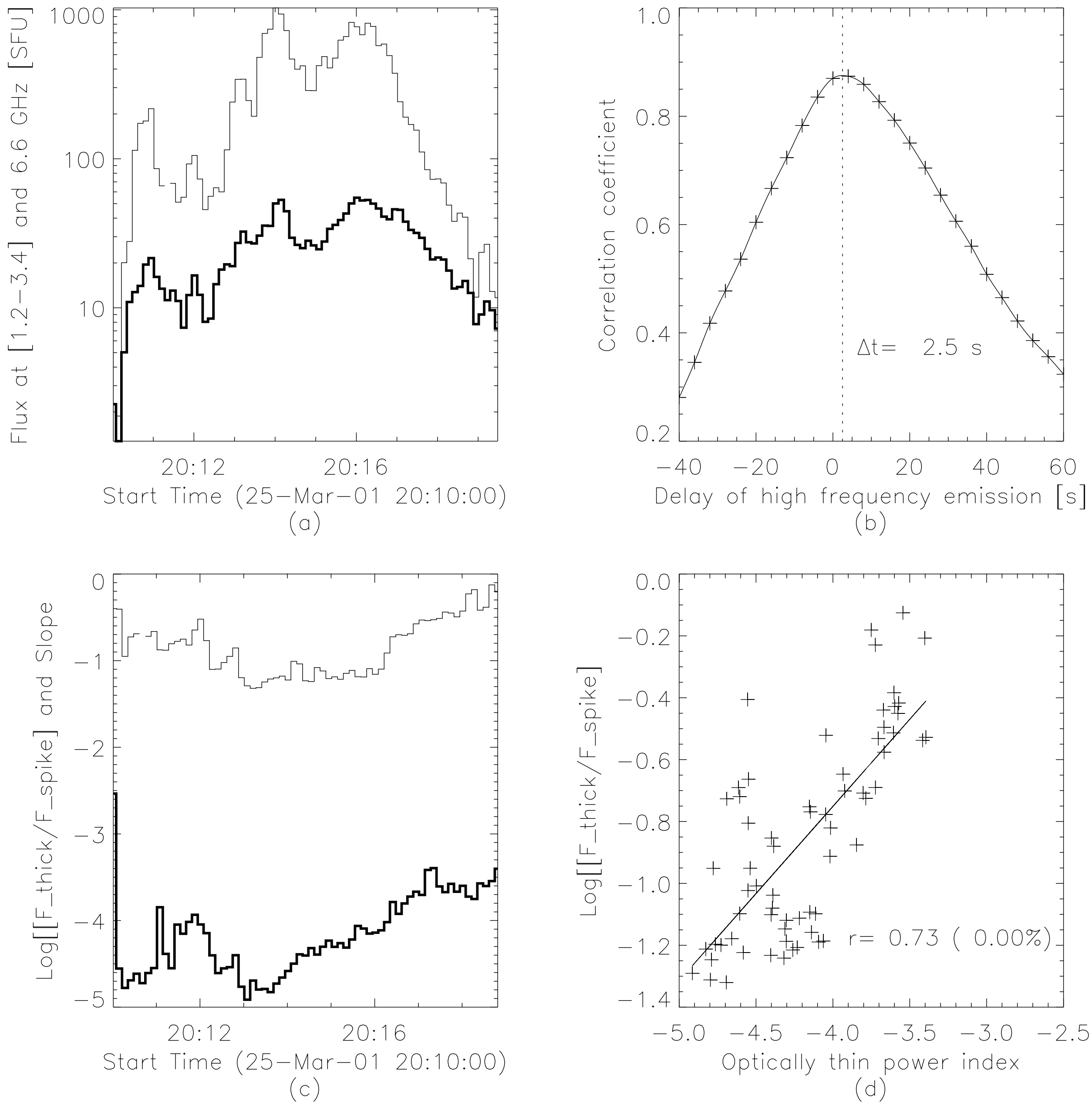

Fig. 3.— March 25, 2001: (a)-Integrated spiky emission over $[1.2 - 3.4]$ GHz (thin line) and the optically thick gyrosynchrotron emission at 6.6 GHz, (thick line). (b)- The linear correlation coefficient (symbols) between the magnitudes displayed in (a) for different time lags. A delay of 2.5 seconds of the high-frequency emission relative to the integrated low-frequency emission has been estimated using a spline interpolation (solid line). (c)- The natural logarithm of the ratio between optically thick and integrated spiky emissions (thin line) and the optically thin spectral index (thick line). (d) The correlation plot of the magnitudes displayed in (c). A linear correlation coefficient of $+0.73$ has been found. The probability for such a correlation coefficient to be the result of a random distribution is 0% to two decimal places.

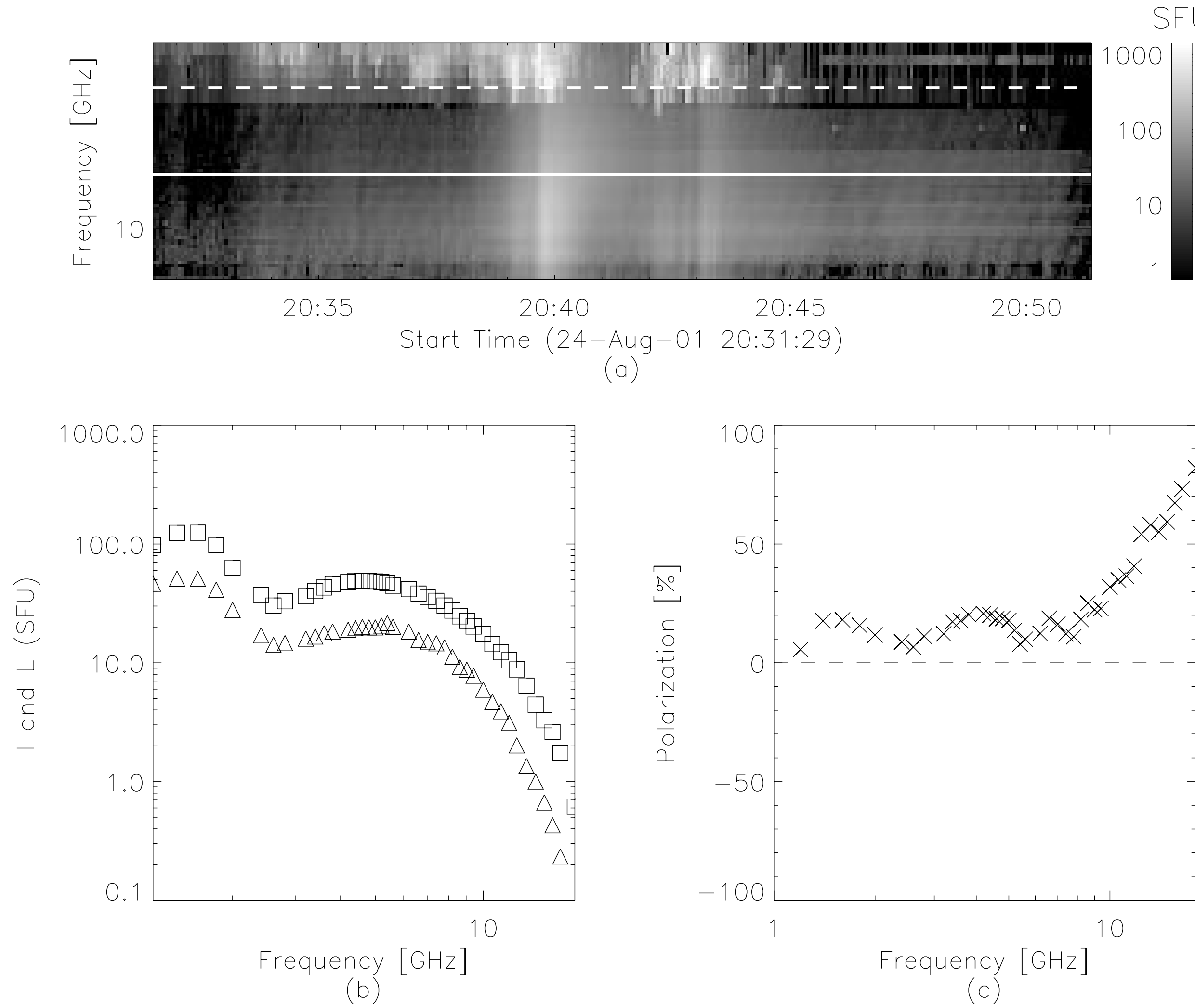

Fig. 4.— August 24, 2001: (a)-Dynamic spectrum recorded by OVSA at 40 frequencies between 1.2 and 18 GHz at 4 s time resolution. The solid line, 5.4 GHz, and the dashed line, 2.0 GHz, represent the optically thick frequency and, respectively, the upper integration limit of the spiky emission used to obtain the results displayed in Fig.5. (b)-The time averaged total power emission (squares) and Left-hand polarization data (triangles) for the same segment of time as in (a). (c)-The averaged polarization spectrum computed using the magnitudes displayed in (b).

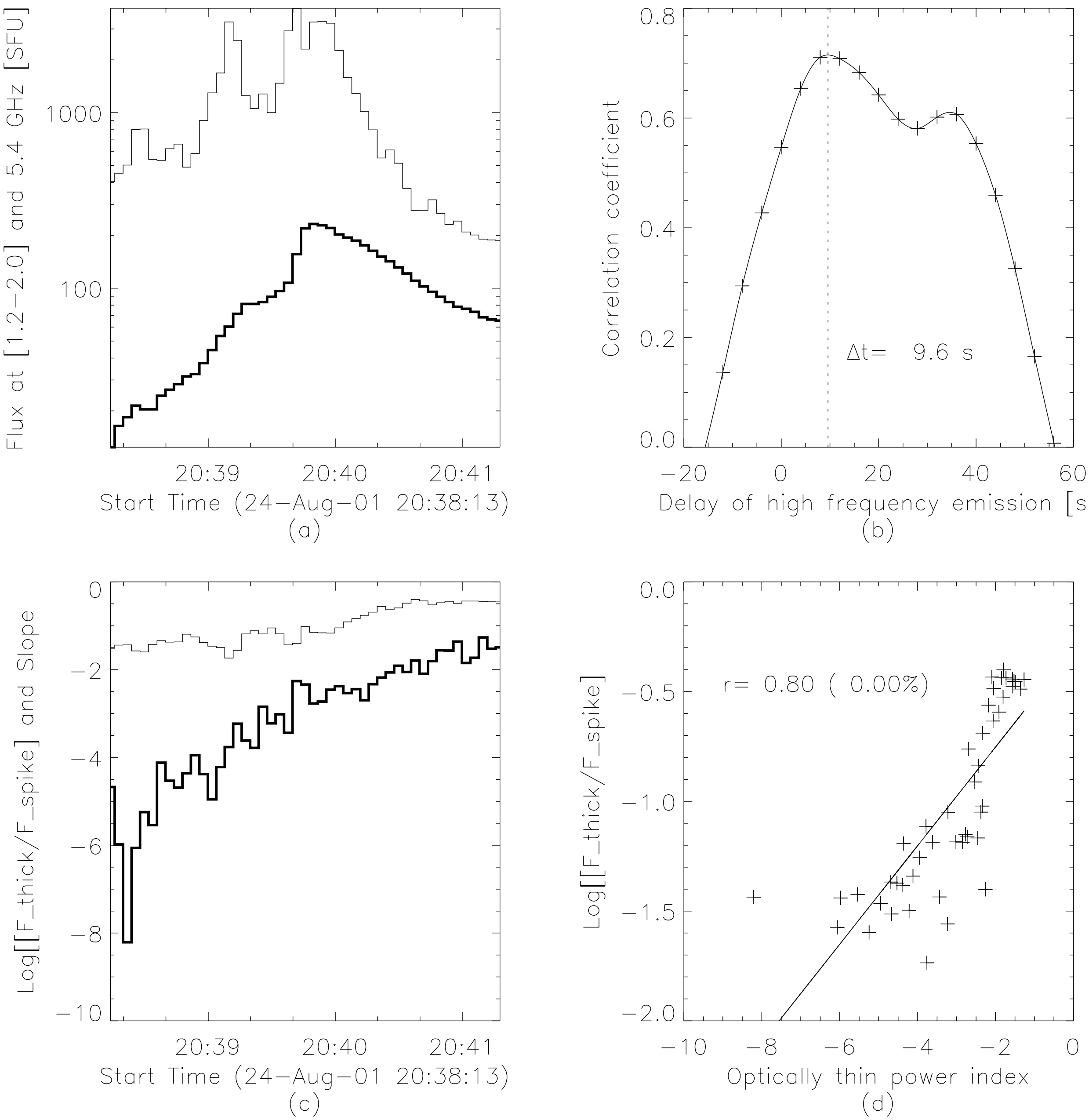

Fig. 5.— August 24, 2001: (a)-Integrated spiky emission over [1.2 − 2.0] GHz (thin line) and the optically thick gyrosynchrotron emission at 5.4 GHz, (thick line). (b)- The linear correlation coefficient (symbols) between the magnitudes displayed in (a) for different time lags. A delay of 9.6 seconds for the high-frequency emission relative to the integrated low-frequency emission has been estimated using a spline interpolation (solid line). (c)- The natural logarithm of the ratio between optically thick and integrated spiky emissions (thin line) and the optically thin spectral index (thick line). (d) The correlation plot of the magnitudes displayed in (c). A linear correlation coefficient of +0.80 has been found. The probability for such a correlation coefficient to be the result of a random distribution is again 0%.

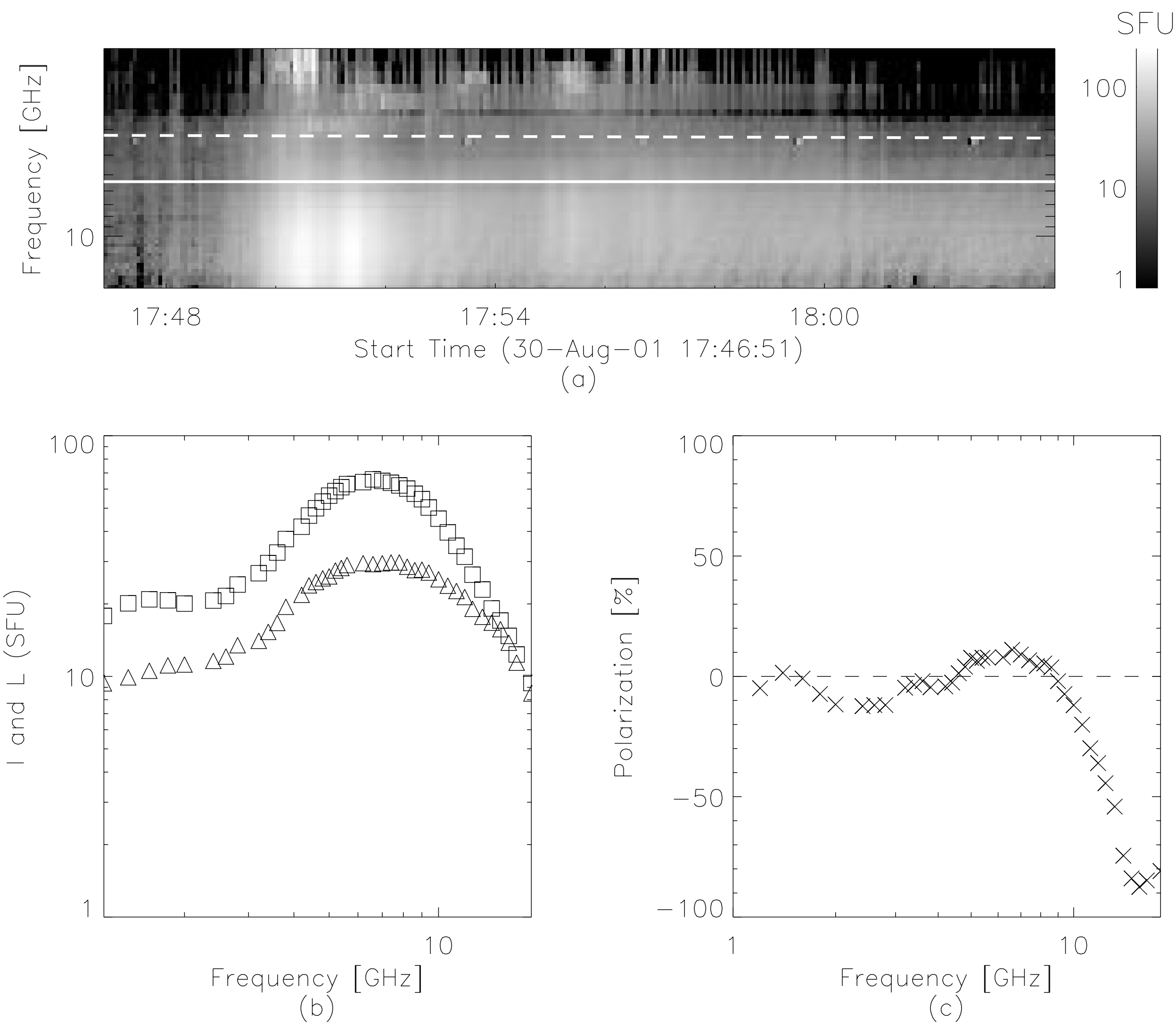

Fig. 6.— August 30, 2001: (a)-Dynamic spectrum recorded by OVSA at 40 frequencies between 1.2 and 18 GHz at 4 s time resolution. The solid line, 5.4 GHz, and the dashed line, 3.2 GHz, represent the optically thick frequency and, respectively, the upper integration limit of the spiky emission used to obtain the results displayed in Fig.7. (b)-The time averaged total power emission (squares) and Left-hand polarization data (triangles) for the same segment of time as in (a). (c)-The averaged polarization spectrum computed using the magnitudes displayed in (b).

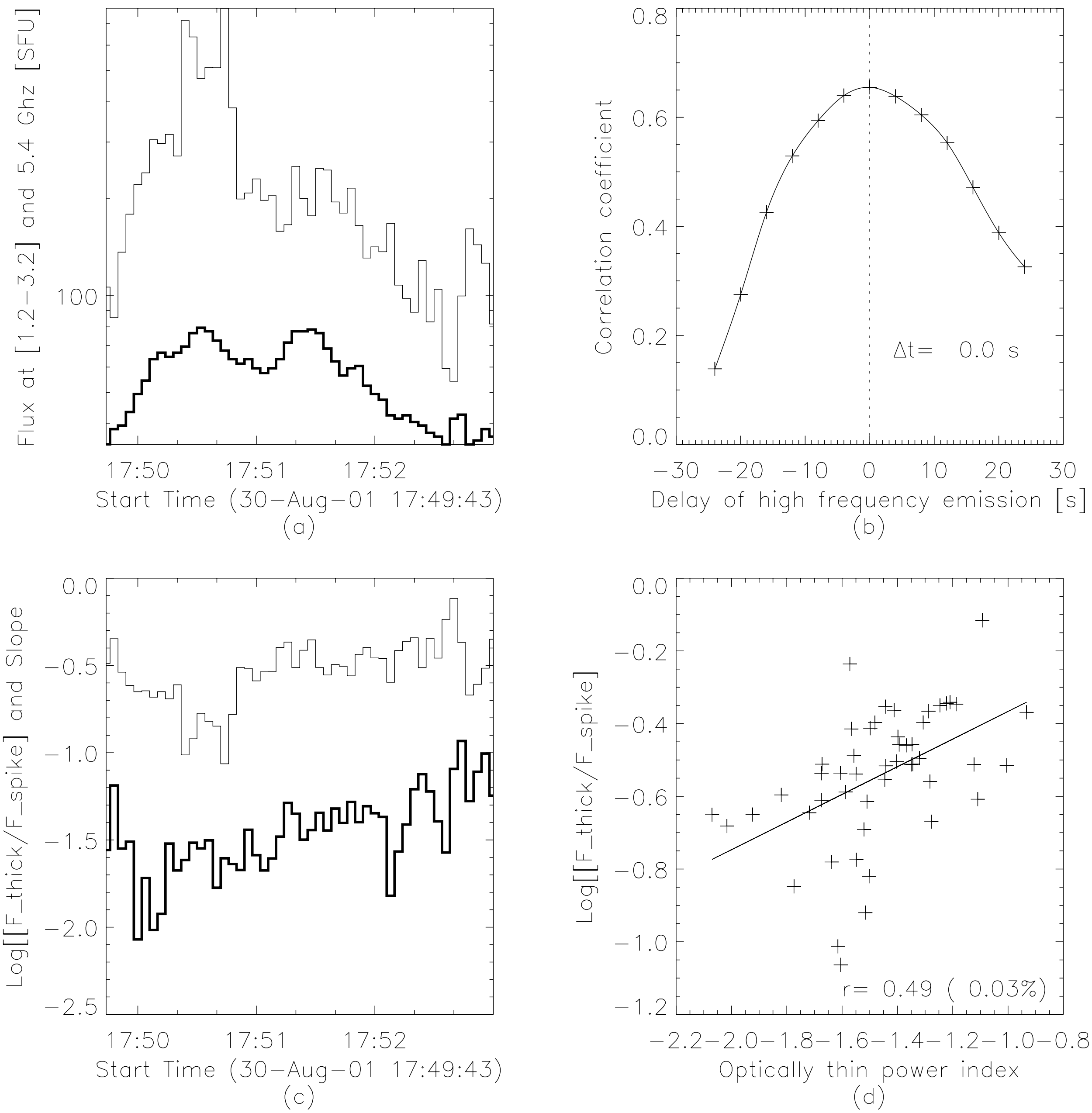

Fig. 7.— August 30, 2001: (a)-Integrated spiky emission over [1.2 − 3.2] GHz (thin line) and the optically thick gyrosynchrotron emission at 5.4 GHz, (thick line). (b)- The linear correlation coefficient (symbols) between the magnitudes displayed in (a) for different time lags. Practically no delay between high-frequency emission and the integrated low-frequency emission has been found in this case. (c)- The natural logarithm of the ratio between optically thick and integrated spiky emissions (thin line) and the optically thin spectral index (thick line). (d) The correlation plot of the magnitudes displayed in (c). A linear correlation coefficient of +0.49 has been found. The probability for such a correlation coefficient to be the result of a random distribution is about 0.03%.

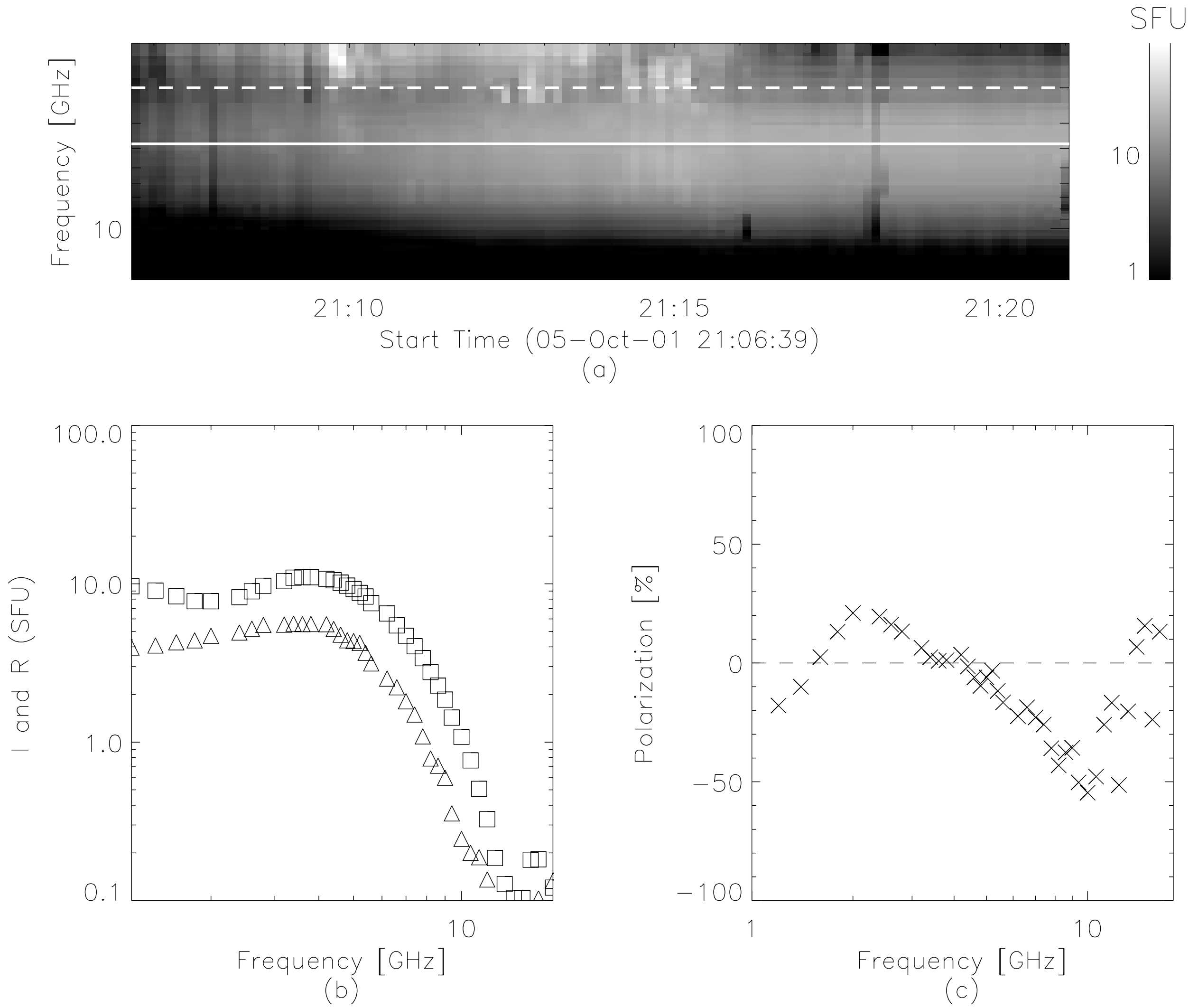

Fig. 8.— October 5, 2001: (a)-Dynamic spectrum recorded by OVSA at 40 frequencies between 1.2 and 18 GHz at 8 s time resolution. The solid line, 3.8 GHz, and the dashed line, 2.0 GHz, represent the optically thick frequency and, respectively, the upper integration limit of the spiky emission used to obtain the results displayed in Fig.9. (b)-The time averaged total power emission (squares) and Right-hand polarization data (triangles) for the same segment of time as in (a). (c)-The averaged polarization spectrum computed using the magnitudes displayed in (b). Only the polarization spectrum below 10 GHz is reliable due to a very weak emision above this frequency, as it can be seen in (b).

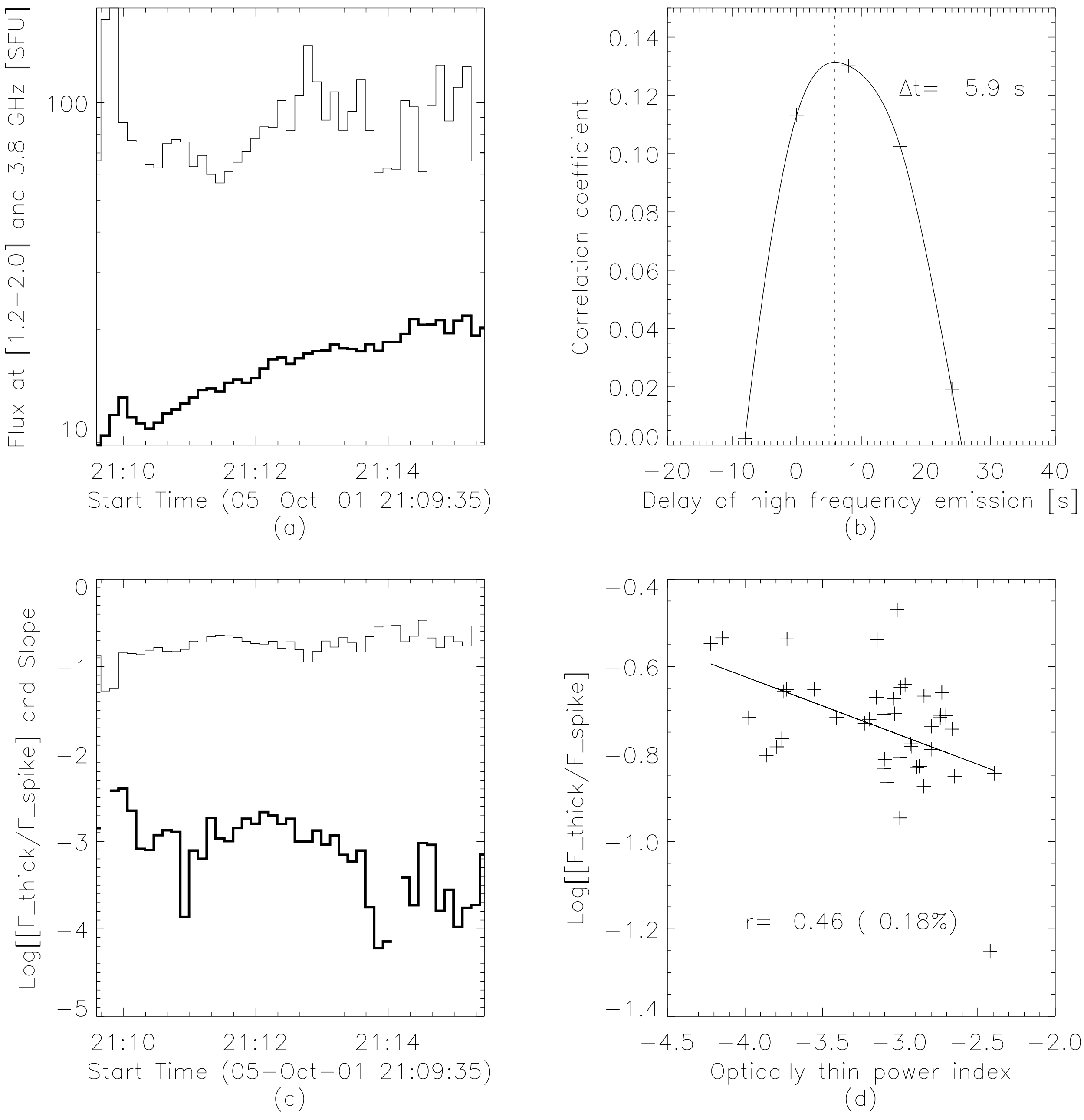

Fig. 9.— October 5, 2001: (a)-Integrated spiky emission over [1.2 − 2.0] GHz (thin line) and the optically thick gyrosynchrotron emission at 3.8 GHz, (thick line). (b)- The linear correlation coefficient (symbols) between the magnitudes displayed in (a) for different time lags. A delay of 5.9 seconds of the high-frequency emission relative to the integrated low-frequency emission has been estimated using a spline interpolation (solid line). (c)- The natural logarithm of the ratio between optically thick and integrated spiky emissions (thin line) and the optically thin spectral index (thick line). (d) The correlation plot of the magnitudes displayed in (c). A linear correlation coefficient of −0.46 has been found. The probability for such a correlation coefficient to be the result of a random distribution is about 0.18%.

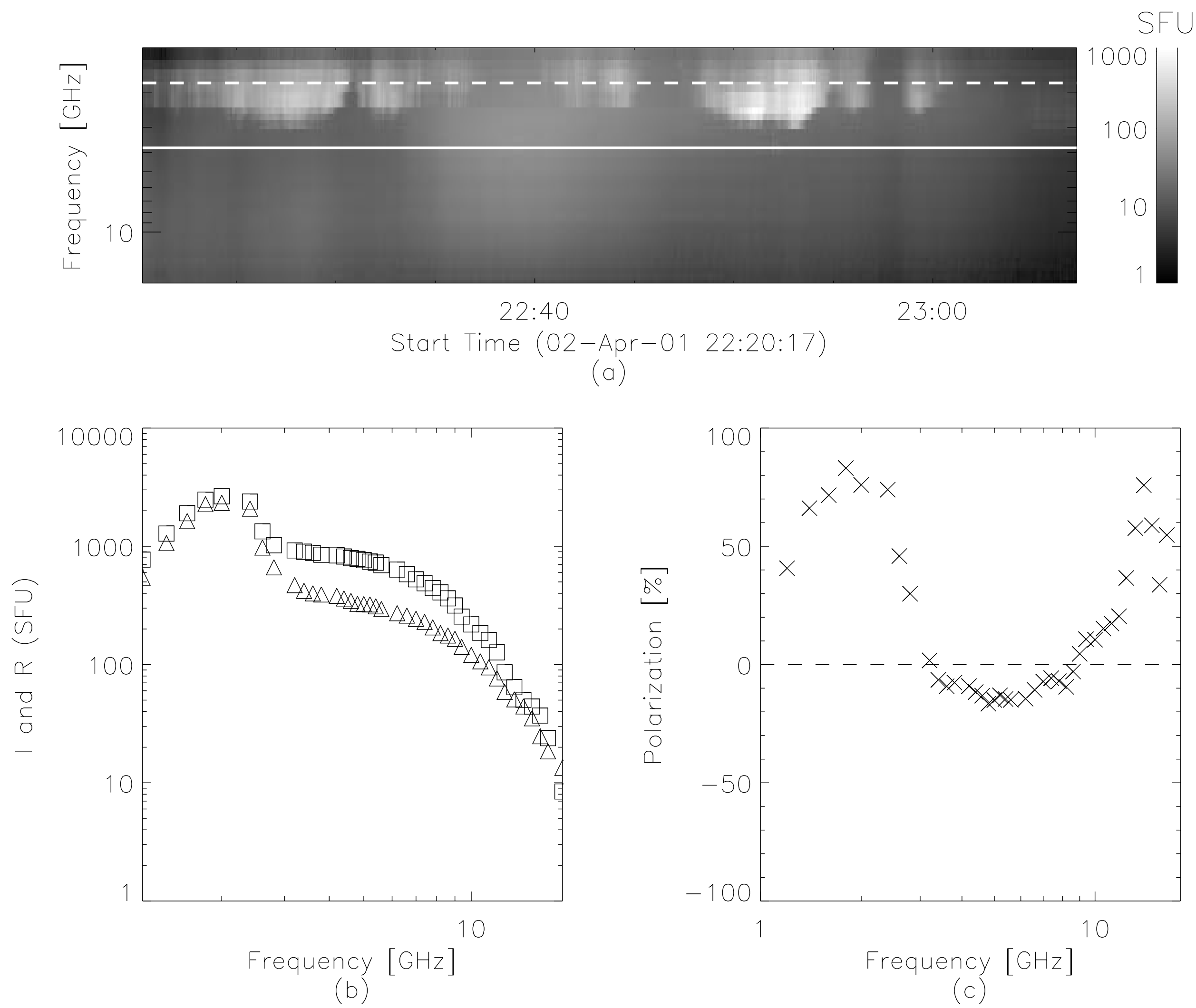

Fig. 10.— April 2, 2001: (a)-Dynamic spectrum recorded by OVSA at 40 frequencies between 1.2 and 18 GHz and 4 s time resolution. The solid line, 3.8 GHz, and the dashed line, 1.8 GHz, represent the optically thick frequency and, respectively, the upper integration limit of the spiky emission used to obtain the results displayed in Fig.11. (b)-The time averaged total power emission (squares) and Right-hand polarization data (triangles) for the same segment of time as in (a). (c)-The averaged polarization spectrum computed using the magnitudes displayed in (b).

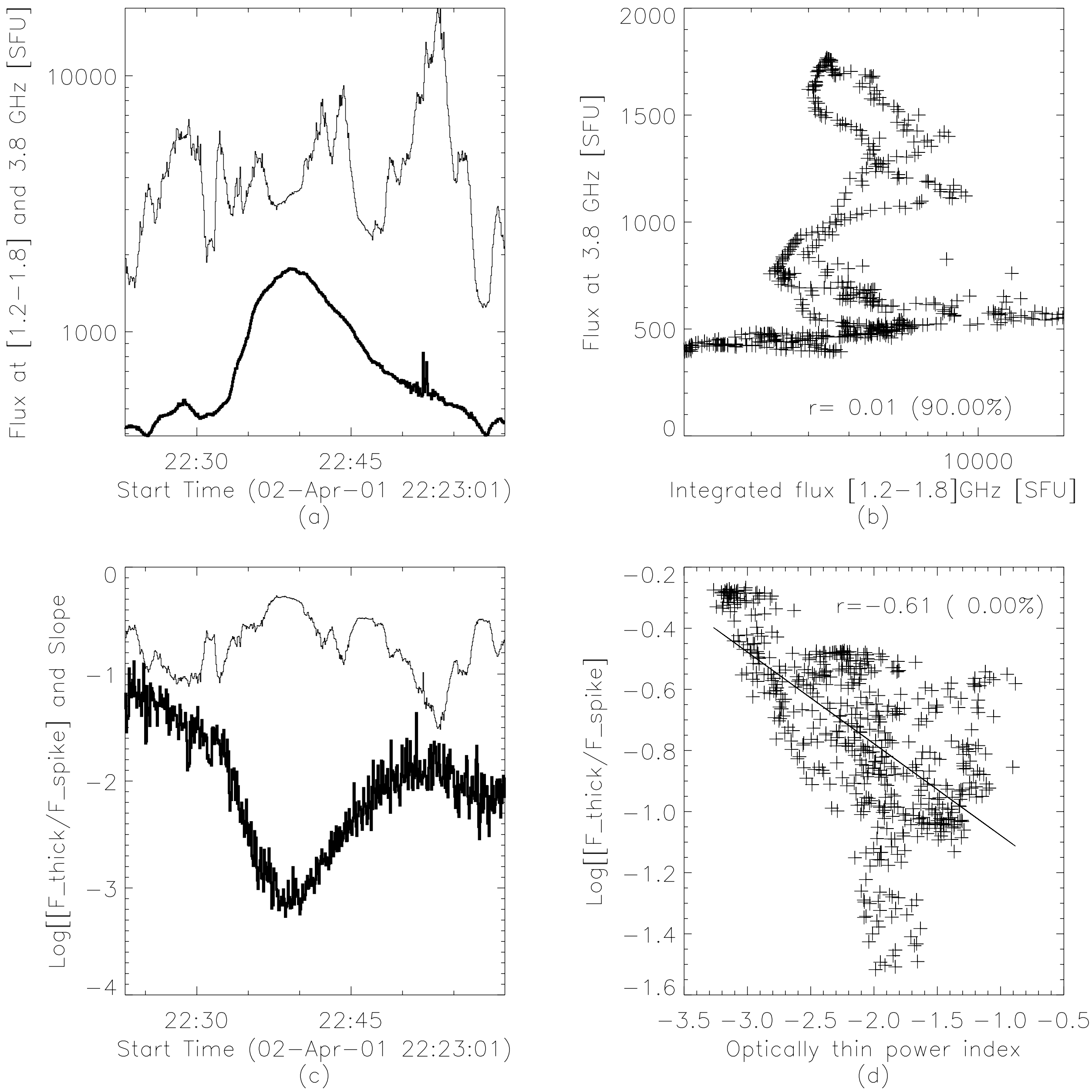

Fig. 11.— April 2, 2001: (a)-Integrated spiky emission over [1.2 – 1.8] GHz (thin line) and the optically thick gyrosynchrotron emission at 3.8 GHz, (thick line). (b)- The correlation plot of the magnitudes displayed in (a). No reliable delay could be found. For the case shown (no time lag) there is practically no linear correlation ($r = 0.01$ corresponding to a 90% probability of a random distribution). (c)- The natural logarithm of the ratio between optically thick and integrated spiky emissions (thin line) and the optically thin spectral index (thick line). (d) The correlation plot of the magnitudes displayed in (c). A linear correlation coefficient of -0.61 has been found. The probability for such a correlation coefficient to be the result of a random distribution is 0% to two decimal places.

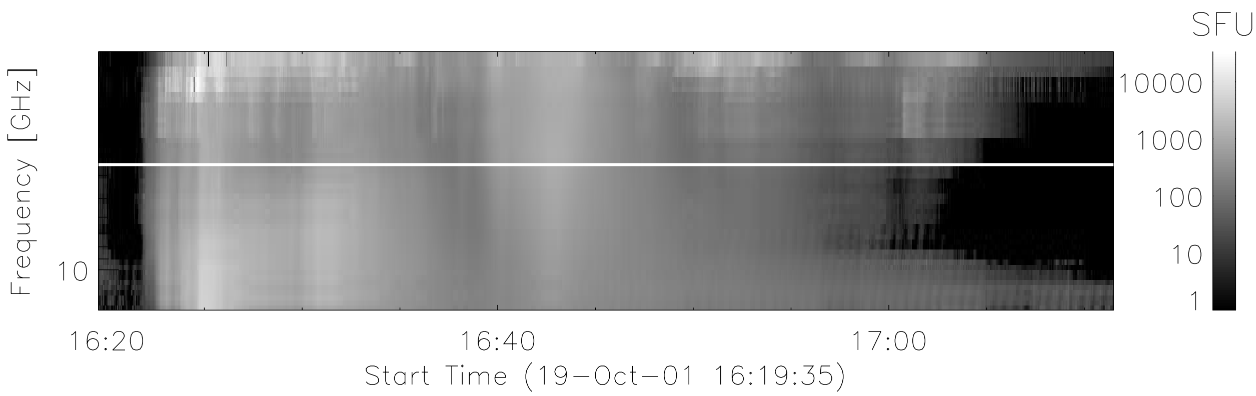

Fig. 12.— October 19, 2001: Dynamic spectrum recorded by OVSA at 22 frequencies between 1.2 and 14.8 GHz and 2s time resolution. The solid line, 3.6 GHz, and the dashed line represents the optically thick frequency used to obtain the results displayed in Fig.13. To analyze the spiky emission only one frequency, 1.2, GHz has been used in this case because a smoothed component becomes important for higher frequencies at the low frequency range. No polarization data are available for this event.

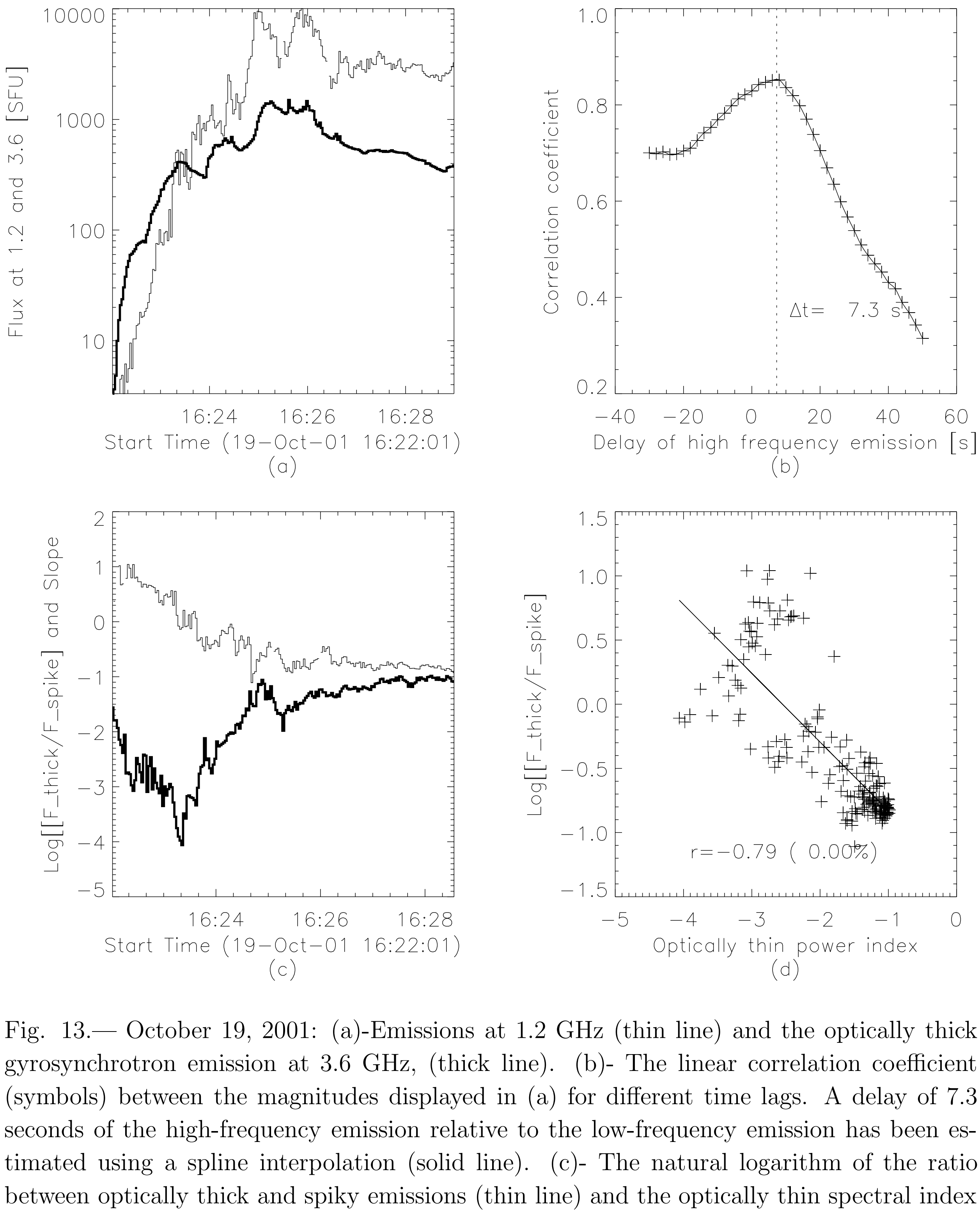

Fig. 13.— October 19, 2001: (a)-Emissions at 1.2 GHz (thin line) and the optically thick gyrosynchrotron emission at 3.6 GHz, (thick line). (b)- The linear correlation coefficient (symbols) between the magnitudes displayed in (a) for different time lags. A delay of 7.3 seconds of the high-frequency emission relative to the low-frequency emission has been estimated using a spline interpolation (solid line). (c)- The natural logarithm of the ratio between optically thick and spiky emissions (thin line) and the optically thin spectral index (thick line). (d) The correlation plot of the magnitudes displayed in (c). A linear correlation coefficient of −0.79 has been found. The probability for such a correlation coefficient to be the result of a random distribution is again 0%.

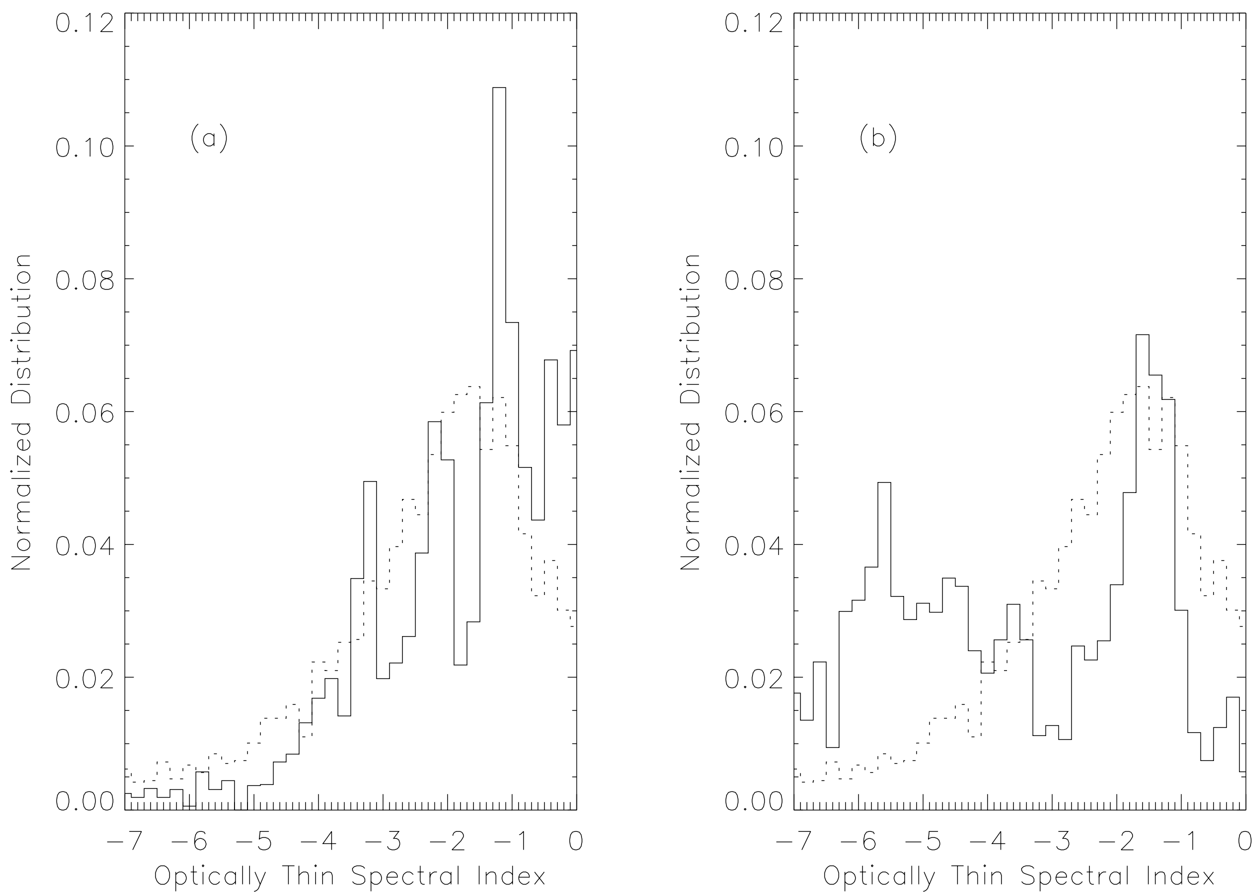

Fig. 14.— (a) Distribution of optically thin spectral index of the presumbly quasitransverse observed spike-producing bursts (solid line). (b) Distribution of optically thin spectral index of the presumably quasiparallel observed spike-producing bursts (solid line). Both distributions are compared with that obtained for 125 gyrosynchrotron bursts above 60 sfu observed by OVSA during 2001 (dashed lines).